Evaporation Peculiarities of Soft Biological Tissues in the Process of Automated 2D-Scanning of CO_2 Laser Radiation

Alexander K. Dmitriev, Alexey N. Konovalov*, Vladimir N. Kortunov, and Valery A. Ulyanov
NRC "Kurchatov Institute",1 Academician Kurchatov Sq., 1123182 Moscow, Russian Federation
*e-mail: ank27.ift@mail.ru

Abstract. The peculiarities of laser evaporation of soft biological tissues in the process of two-dimensional scanning of continuous CO_2 laser radiation were studied experimentally and numerically. Samples from agar and pig heart muscle in vitro were used as soft biotissue models. The depth of evaporation and the peculiarities of the formed surface of the evaporated zone were studied for different regimes of exposure: radiation power, scanning speed of the laser beam, filling density of the scanned zone. A semi-empirical model of laser evaporation of soft biological tissues with high water content is proposed based on the energy balance and the evaporative mechanism of biotissue removal. Studies have shown good agreement between experimental data and data obtained based on the proposed model. © 2024 Journal of Biomedical Photonics & Engineering.

Keywords: CO_2 laser; automated scanning; precision evaporation; biomodel; robot-assist surgery.

Paper #9115 received 7 Jun 2024; revised manuscript received 1 Oct 2024; accepted for publication 1 Oct 2024; published online 10 Nov 2024. doi: 10.18287/JBPE24.10.040307.

1 Introduction

The use of robotic and automated devices and systems in surgery is one of the promising areas for developing and improving the current medical technologies [1−3]. This approach reduces the risks of the human factor, decreases the time of surgical intervention, increases the efficiency and safety of treatment, and allows for rapid postoperative rehabilitation of patients.

High-precision and low-trauma laser surgical interventions have led to widespread devices based on CO_2 lasers with scanning systems. These devices make the process of exposure to laser radiation automatic [4]. CO_2 lasers still remain the most common in global medical practice and are most commonly used for the so-called ablative (local evaporation of tissue) or non-ablative (local heating of tissue) laser skin resurfacing [5, 6]. This technology is considered the gold standard in dermatological surgery. Currently, active research is being conducted on the use of scanning laser systems in relation to the problems of obtaining precision cuts of complex shapes of a given depth and evaporation of a given area of arbitrary shape on the biotissue surface. The scanning systems can effectively control the parameters of laser radiation in the impact zone. They provide high speed and accuracy, safety and reproducibility of operations using CO_2 lasers [7]. This significantly expands the possibilities and prospects for their use in surgery.

One of the directions in the development of robot-assisted laser surgery is predictive modeling for the purpose of preoperative planning [8, 9]. Planning is based on the selection of the optimal modes of automated laser exposure, ensuring high efficiency of the laser procedure. These approaches to carrying out precision and low-trauma laser operations are based on experimental and numerical modeling of laser irradiation processes using various *in vivo* or *ex vivo* biomodels. Ref. [10] suggests selecting the modes and predicting the depth of automated laser incision of soft tissues by means of an experimental database. To this end, they used *ex vivo* chicken muscle tissue. The obtained accuracy of the depth of the cut reached accuracy of ±100 μm. In Refs. [11, 12], to achieve a given depth of laser evaporation of soft and bone tissues, it is proposed to use simplified mathematical models for predicting the depth of the cut using experimental data on animal tissues. Ref. [13] proposed a method for simulating the removal of the superficial tumors while minimizing the damage to the healthy tissue with the help of a laser beam whose profile corresponds to the 3D shape of the pathological tissue. It is noted in Refs. [9, 14] that in the long term, the development of the robot-assisted laser surgery will

require developing predictive models of the interaction between laser radiation and various types of tissues.

An analysis of modern trends in the development of laser surgery shows that the creating of models of laser evaporation of biological tissue is urgent task due to development of robotic automated surgical complexes [9, 14]. There are numerous works devoted to modeling laser thermal and destructive effects on biological tissue. Usually such studies investigate the threshold conditions for laser destruction of biological tissue [15] and the features of its thermal damage [16], describe the formation of temperature fields during laser action and explosive boiling of interstitial fluid [17−19], and the generation of laser-induced mechanical stresses [20]. The overwhelming majority of studies are devoted to laser evaporation of biotissues in the short-pulse mode. There are much fewer works that study the effect of continuous laser radiation on biotissues. There are also few works that model the depth of cut and the depth of evaporation of the tissue zone during two-dimensional scanning of continuous laser radiation. There are known works [10, 12], which propose a completely empirical approach to predicting the depth of automated linear cutting of soft biotissues by continuous CO_2 laser radiation. Samples from agar and chicken muscle tissue were used as biomodels. This approach is based on a linear approximation of experimental data by the parameter of the input energy and the exposure time. These works do not analyze the features of the influence of the laser beam scanning speed. There is also no physical model that would allow the surgeon to predict the result of cutting and evaporation of a two-dimensional tissue zone in relation to a laser installation that has its own specific parameters of the laser beam and scanning system (spot diameter, scanning speed, etc.).

The purpose of this work is an experimental and numerical study of the efficiency and characteristics of the evaporation of soft biological tissues in the process of automated two-dimensional scanning of CO_2 laser radiation. A physical evaluation model of the depth of the evaporated region of soft biological tissue with high water content is proposed depending on the modes of two-dimensional laser scanning and the parameters of the laser beam.

2 Methods and Materials

For automated surface laser evaporation of biomodels, we used a setup consisting of a laser unit, an articulated-mirror manipulator and a 2-coordinate galvanic *Galvo Scanner*, Model *JS*1105 (*Sino-Galvo Technology Co.*, China) coupled to it. The setup is based on the *C*-20*A* single-mode CO_2 laser (*Coherent*, USA) with a power up to 20 W. A detailed description of the setup is given in Ref. [21].

The scanner control unit and the specially developed software make it possible to set any shape of the evaporation area within 20 × 20 mm, the speed of the laser beam within 1–50 mm/s, and the required filling density of the evaporated surface by laser hatching. The surface scanning area is a set of parallel lines (hereinafter, 'hatching lines'). The required density of filling the evaporated area of the surface by laser hatching was secured by changing the distance between the hatching lines.

The samples based on *Difco*™ agar and pig heart muscle tissue *in vitro* were used as biomodels. Biotissues were used within 48 h *post mortem.* The samples were stored at the temperature of 0–4°C with constant humidity. The heart muscle was used for the following reasons. Firstly, it is known that pig tissues are most similar in their parameters to human ones and are used in modeling surgical processes. Secondly, relatively large areas of tissue that would be homogeneous could be found quite easily in the heart muscle. Other soft tissues are much less homogeneous. For example, skeletal muscles often contain ligaments, fat, vessels, and tendons. This would significantly complicate the experiments and analysis of the data obtained. For experiments with agar, the prepared samples contained 15% agar mass fraction and 85% water fraction. These samples simulated soft water-containing tissues. The cross sections of biomodels were studied under a digital USB microscope (magnification 10x−200x, resolution 1600 × 1200, China).

In experiments on automated evaporation of the biomodel surface areas, a single scan of the rectangular area measuring 8.5 mm × 11.6 mm was performed (the lens focal length = 50 mm). The radiation was focused onto the surface of the biomodel. The focal spot size was 175 μm at the 86% level. During the experiments, some exposure and scanning modes were changed: the power of laser radiation (2–5 W), the speed of the laser beam (from 2 mm/s to 20 mm/s), the density of filling the evaporated area of the surface of the biotissue by hatching. The distance between the hatching lines ranged from 75 to 450 μm.

3 Results

Laser evaporation of the surface of agar samples was studied in accordance with the filling density of the hatching and scanning speed. At low filling density of the scanned area, the surface of the evaporated zone has a sawtooth shape. At a high filling density of the area (the distance between the hatching lines equal to or less than the width of the evaporated channel), the surface of the evaporated region of the sample is smoother and more uniform than at a low filling density. A similar result is achieved by decreasing the scanning speed at a fixed distance between the hatching lines. Fig. 1 shows cross sections of agar samples after evaporation for scanning speeds of 12.5 mm/s, 9 mm/s and 4.5 mm/s and the distance between hatching lines of 450 μm. As follows from the figure, at the scanning speed of 12.5 mm/s, the surface has a sawtooth shape, whereas at the scanning speed of 4.5 mm/s, the surface becomes smoother. This is due to the fact that as the scanning speed decreases, the width of the evaporated channel increases, since the thermal front has time to spread over a greater distance. As a result, the evaporated surface is smoothed due to the overlap of adjacent hatching channels. This is similar to what happens when the distance between the hatches is reduced.

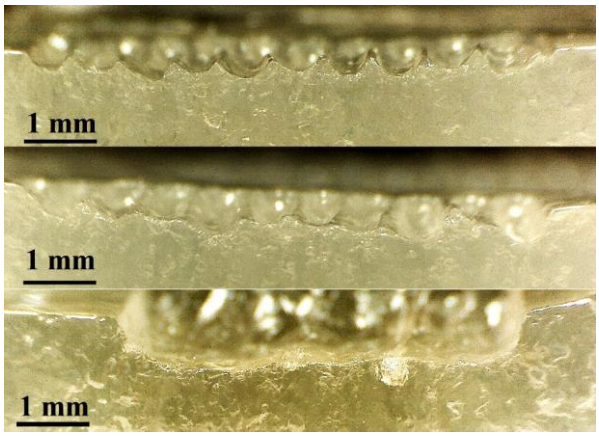

Fig. 1 Cross section of the evaporated zone in the agar samples under various single-pass scanning modes: P = 4 W; the distance between hatching lines = 450 μm; the scanning speed (top to bottom): 21; 14.5, and 7.4 mm/sec.

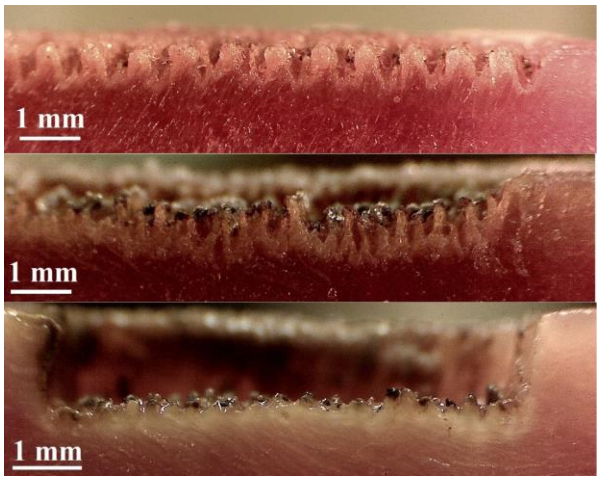

Fig. 2 Cross section of the evaporated zone of the cardiac muscle at P = 3.6 W: (a) d = 0.445 mm, V = 7 mm/s, (b) d = 0.150 mm, V = 7 mm/s, (c) d = 0.75 mm, V = 11.3 mm/s.

The experiments have also demonstrated that the depth of the evaporated zone increases both with increased hatching density and with decreased scanning speed. This is due to the fact that the energy input per unit area increases both at a lower scanning speed and at a filling density with hatching.

A similar picture was observed when evaporating the biomodels based on the cardiac muscle (Fig. 2). The main difference was that with denser hatching, the surface of the evaporated hangar area is significantly greater even compared to the heart muscle. This may be caused by the fact that when melting, agar acquires a smoother surface. Secondly, there is a change in the color of the tissue in the vaporized area on the surface of the heart muscle samples, which is caused by coagulation and carbonization of the tissue at high temperatures. For the agar samples, this effect was not observed.

In the general case, the surface of the evaporated zone of biomodels is uneven due to scanning and the peculiarities of the thermophysical processes in the irradiation zone. In the evaporated zone, a change in depth is observed from a certain minimum value H_{min} to a maximum H_{max} (Fig. 3). It is clear that the average value of the depth <H> of the evaporated zone is determined by the average value of the deposited energy by laser radiation (for more details, see Section "Model of soft tissue evaporation"). Due to the difficulty of determining <H> from the photographs of cross sections, we characterized the result of evaporation during laser scanning by the maximum depth H_{max}.

Fig. 4 shows the relationship between H_{max} and the scanning speed V for different biomodels. As can be seen from the figure, the depth of evaporation of agar and the cardiac muscle is almost the same. This was to be expected, since the determining factor in such biomodels is the absorption of radiation by water at the wavelength of 10.6 μm. The agar-based samples present a fairly good model of soft tissue from the point of view of assessing the effectiveness of laser evaporation.

Fig. 5 shows the relationship between the evaporation depth and the laser radiation power. The obtained data fits well with the linear relationship. This suggests that the determining factor is the input laser energy.

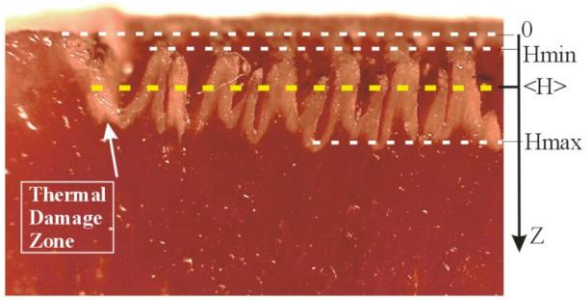

Fig. 3 Cross section of the evaporated zone of the cardiac muscle at P = 3.55 W, V = 3.5 mm/sec, d = 0.445 mm.

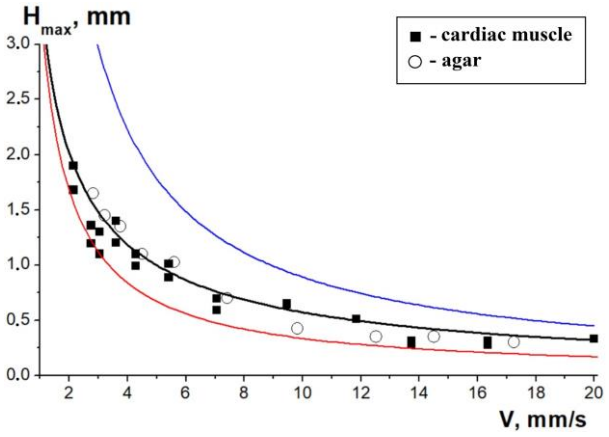

Fig. 4 The relationship between the evaporation depth of biomodels and the scanning speed V, d = 0.445 mm. The red curve is the average depth <H>, the blue curve is without taking into account thermal conductivity, the black curve is taking into account thermal conductivity (χ = 1.2 10^{-7} m^2/s).

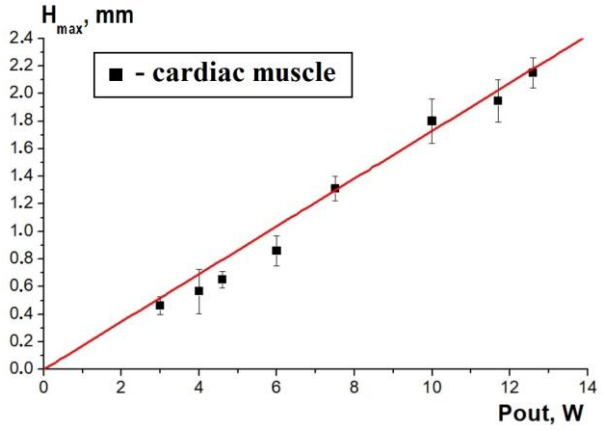

Fig. 5 The relationship between evaporation depth of cardiac muscle H_{max} and the radiation power. V = 15 mm/s, d = 0.15 mm. The red line represents the calculated linear relationship between the average evaporation depth of cardiac muscle and the power according to Eq. (7).

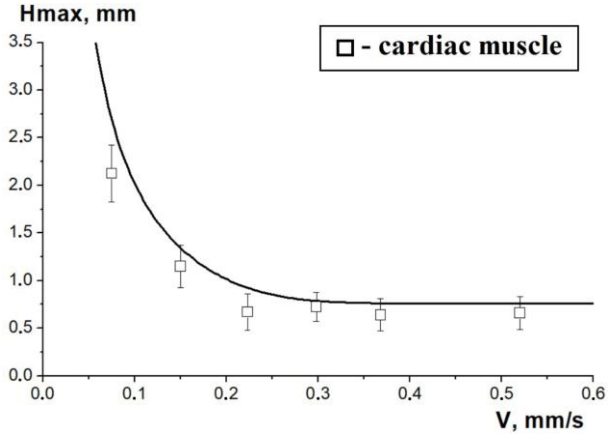

Fig. 6 The relationship between H_{max} and distance d between the hatching lines at the scanning speed of 7 mm/s. The black curve represents calculation taking into account thermal conductivity (χ = 1.2 10^{-7} m^2/s).

Fig. 6 shows the relationship between the maximum evaporation depth H_{max} and distance d between the hatching lines at the scanning speed of 7 mm/s. A rapid increase in the evaporation depth is observed with decreased distance d. As d increases, there is no change in the evaporation depth. This is due to the fact that at large distances d, scanning turns into separate cuts whose depth is constant and depends only on the scanning power and speed.

4 Model of Soft Tissue Evaporation

For soft biotissues with high water content (70−80% and more), we propose a semi-empirical model that allows determining the depth of the evaporated area of biotissue during laser scanning with continuous CO_2 laser radiation. This model assumes that the process of biotissue evaporation by continuous radiation occurs far beyond the threshold of the onset of evaporation. In this case, the intensity of the laser energy input is such that the interstitial water reaches the boiling point and higher. This leads to its intensive evaporation, accompanied by microexplosions with the mass removal from the impact zone. The model is based on the energy balance, taking into account that almost all the energy of laser radiation input into the tissue is spent on the vaporization of the water contained in it.

To justify this assumption, we will conduct some assessments. First, let us make an assessment of the threshold at which water begins to boil. The rate of temperature rise in the center of the laser spot at the initial moment of time, when the thermal conductivity is negligible, can be defined as:

$$\frac{dT}{dt} = \frac{P\mu_a}{\pi\rho C r_0^2}, \quad (1)$$

where $P = P_0 \cdot (1-R)$, P_0 – laser radiation power, R – reflection coefficient from the tissue surface, r_0 is the radius of the laser beam, ρ, C, μ_a density, specific heat and absorption coefficient for biotissue.

In this paper, only soft tissues with high water content are considered. In this regard, for further estimations we will take the values of thermophysical characteristics for water: $\rho = 10^3$ kg/m^3 and C = 4200 J/kg. The presented model does not take into account light scattering, since the determining factor in the propagation of 10 μm radiation in soft tissues is the high absorption of water. In this regard, to estimate the absorption of soft tissue, we will use the absorption coefficient for water μ_a = 792 cm^{-1} [22].

The rate of temperature rise during the passage of a laser beam with scanning speed V can be approximately estimated as follows:

$$\frac{dT}{dt} = \frac{\Delta T}{2r_0/V} = \frac{P\mu_a}{\pi\rho C r_0^2}. \quad (2)$$

From this relationship, we obtain the water boiling (ΔT = 100 °C) threshold power for a given scanning speed:

$$P_{th} = \frac{\pi\rho C r_0 V \Delta T}{2\mu_a}. \quad (3)$$

From Eq. (3) we obtain that at the scanning speed of 10 mm/s and the beam radius of 90 μm, the power threshold for boiling point is 11 mW. This estimate is made under the assumption that during the time $2r_0/V_0$, the thermal front propagates over a distance that is significantly shorter than $1/\mu_a$. This is true for the scanning speed $V_0 >> 2r_0\chi\mu_a^2$ = 27 cm/s. At speeds lower than this value, the thermal front spreads over the distance of $\Delta z = (\chi 2r_0/V_0)^{0.5}$ in the time interval of $2r_0/V_0$. From energy considerations it is easy to obtain the boiling threshold for this case:

$$P_{th} = \frac{\pi\rho C r_0 V \Delta T}{2}\left(\frac{1}{\mu_a} + \sqrt{\frac{2r_0}{V}\chi}\right). \quad (4)$$

At V = 10 m/s and r_0 = 90 μm, the threshold power will be P_{th} = 39 mW. The estimates have shown that for both high and low scanning speeds, the water boiling power threshold is significantly smaller than 1 W.

Thus, when soft biological tissues are exposed to radiation power of one W or above at the wavelength of 10.6 μm, the temperature in the exposure zone quickly reaches the boiling point. Upon reaching this temperature, the process of intense evaporation of water begins. The excess energy deposited in the laser radiation zone is no longer spent on heating but on the vaporization process. This is accompanied by micro-explosions and the removal of vapor-droplet mixture from the impact zone [23, 24]. In this model, we also assume that the mechanical energy associated with the removal of mass from the impact zone is negligible (this will be shown below after obtaining the estimates of the evaporation depth). Thus, for this model, it is assumed that the removal of tissue volume is determined solely by vaporization.

Using this assumption, it is possible to obtain the average depth of the evaporated zone when scanning a laser beam. Let laser scanning be carried out at the speed V of the rectangular zone of dimensions $L \times M$, along the face of length M. Let the distance between the hatching lines be d. In this case, the total scanning time will be $\Delta t = (M\cdot(L/d)+L)/V$. From the condition that all the adsorbed energy is spent on evaporation, it turns out:

$$P\Delta t = \rho QLM\langle h\rangle, \tag{5}$$

where $\langle h\rangle$ is the average depth of the evaporated zone and $Q = 2.26\cdot10^6$ J/kg represents specific heat of vaporization. Assuming that $M >> d$, we obtain the average depth of the evaporated zone:

$$\langle h\rangle = \frac{P}{\rho QVd}. \tag{6}$$

It is clear that when $d >> r_0$, the result of scanning will not be an evaporated layer of tissue, but individual cuts in the area of the rectangular scanning zone. In this case, the average depth taken over the scanning area $L \times M$ will also be equal to $\langle h\rangle$.

Let us assume that all the evaporated tissue of layer $\langle h\rangle$ was removed from the impact zone at speed u. Then the mechanical energy will be equal to $E_m = \rho\langle h\rangle M\cdot Lu^2/2$. The energy delivered to the biological tissue when scanning the area $M\cdot L$ is equal to $E_{las} = P\,\Delta t$. The ratio of the mechanical energy of mass removal to laser energy, taking into account Eq. (6) will be: $E_m/E_{las} = u^2/(2Q)$. Even if we take a sufficiently high mass removal rate of 10 m/s (the characteristic velocity of 1–3 m/s [23, 24]) for estimation, we obtain a fairly small value of $E_m/E_{las} = 3.8\cdot10^{-5}$ ratio of the mechanical energy to the delivered laser energy during evaporation of layer $\langle h\rangle$.

Thus, the accepted approximation that mechanical energy of mass removal and thermal energy can be neglected is satisfied quite well. Fig. 5 shows the linear dependence of $\langle h\rangle$ on the radiation power at a scanning speed of 15 mm/s and the distance between lines d = 0.15 mm. The figure demonstrates a fairly good agreement with the experiment. At the same time, the value of the average evaporation depth $\langle h\rangle$ is not quite suitable for characterizing the scanning result with relatively sparse hatching ($d > r_0$). For example, photographs of sections of an evaporated myocardial sample show explicit laser cuts (Fig. 2 and Fig. 3). A simple calculation of one value $\langle h\rangle$ is not very informative in cases where the average evaporation depth $\langle h\rangle$ is less than or comparable to the cutting depth. Fig. 4 shows the evaporation depth as a function of scanning speed at radiation power P = 3.55 W and d = 0.445 mm. The difference between the calculated curve of the average evaporation depth (Eq. (6)) and the measured values is quite strong. This is due to the fact that the measurements were taken not for the average evaporation depth but for the maximum depth H_{max} that is observed in the scanning area. With a relatively sparse hatching, this value H_{max} is greater than the average evaporation value over the entire scanning area.

To describe of this process in more detail, the shape of the channel during cutting and the overlap of these cuts with each other at $d < r_0$ must be taken into account. This can also be done under the assumption that all energy goes into evaporation. Let us consider a single cut of length M, which is obtained when a laser beam passes at a speed V.

Then, pertaining to energy, we find that the energy deposited during the passage of the laser beam at distance M was spent on evaporating water with volume $M\cdot S_0$, where S_0 is the cross-section area of the resulting channel. Thus we get:

$$S_0 \equiv \int_{-\infty}^{\infty} h(x)dx = \frac{P}{V\rho Q}, \tag{7}$$

where $h(x)$ is the shape of the cross-section of a separate cut.

In our model, the depth of the evaporated zone is determined by the absorbed energy. Therefore, at high scanning speeds, when the thermal front extends over a distance significantly less than the beam radius during $2r_0/V$, the depth $h(x)$ will repeat the shape of the laser beam profile. If the laser beam has a Gaussian shape, then $h(x)$ will also have a Gaussian shape:

$$h(x) = H_0 e^{-\left(\frac{x}{r_0}\right)^2}. \tag{8}$$

From energy considerations it is easy to obtain that:

$$H_0 = \frac{P}{\sqrt{\pi}V\rho Q r_0}. \tag{9}$$

According to energy considerations, the resulting shape of the evaporated layer will be the sum of depths $h(x)$ for all hatching lines of the evaporated zone $L\times M$ that are located equidistantly with a period d:

$$H(x) = \sum_{k=0}^{N} h(x - kd), \quad (10)$$

where $N = int(L/d)$ is the number of hatching lines in the evaporated zone (*int* is the integer part of the division).

Knowing the profile of an individual cut $h(x)$, it is easy to calculate the profile of the entire evaporated zone for different scanning parameters. Fig. 7 shows shapes $H(x)$ of the evaporated layers at various distances between the hatches at the scanning speed of 7 mm/s with the Gaussian shape of a single laser channel.

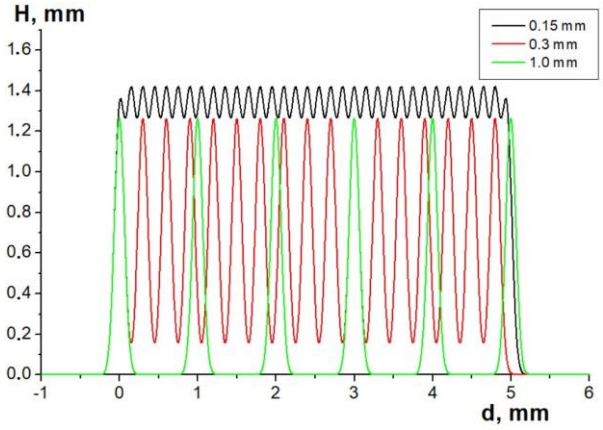

Fig. 7 Shapes $H(x)$ of the evaporated layers at various distances between hatches. V = 7 mm/s.

These dependencies can find the average depth and maximum depth in the evaporation zone. Numerical modeling has shown that the average depth $<H>$ calculated as the average of function $H(x)$ coincides with the average depth calculated using the simplified model (Eq. (6)). Fig. 4 shows the relationship between the maximum evaporation depth (blue line) and the scanning speed at the distance between the hatching lines of 0.445 mm. As can be seen from the figure, the calculated value H_{max} significantly exceeds the experimentally measured value. This is due to the fact that a Gaussian function with a half-width equal to the radius of the laser beam was taken as the profile of a single cut $p(x)$. In reality, this is not true, since during the movement of the beam over a distance equal to the diameter of the laser spot, the thermal front spreads over the distance of $\Delta x = (\chi 2r_0/V_0)^{0.5}$. As a result, the width of the evaporation zone can differ from the diameter of the laser beam. The lower the scanning speed, the wider the evaporation zone will be due to heat propagation.

Taking into account this factor, we assumed that in the presence of thermal conductivity, the profile of a single cut also retains the Gaussian shape, but the half-width of the Gaussian profile r_{eff} due to heat transfer depends on the scanning speed as follows:

$$r_{eff} = r_0 + \sqrt{\frac{2r_0}{V}\chi}. \quad (11)$$

By substituting the value of the effective radius r_{eff} in Eq. (8) instead of r_0, we can recalculate the maximum evaporation depth as a function of speed. Fig. 1 shows the relationship between H_{max} (black line) and the scanning speed when thermal conductivity is considered. Here we can see a fairly good agreement with the experimental data.

Fig. 6 shows the relationship between H_{max} and distance d between the hatching lines at the scanning speed of 7 mm/s in the presence of thermal conductivity. The peculiarities of the dependence of H_{max} on parameter d are explained by the fact that at large distances d, individual tissue cuts occur and their depth is determined only by profile $h(x)$. With denser hatching, profiles $h(x)$ overlap and the depth increases due to the summation of profiles for individual cuts (Eq. (10)).

As can be seen from Fig. 6, the calculated curve of H_{max} versus d also correlates well the experiment. Thus, the proposed model demonstrates a good agreement with the experiment on the maximum evaporation depth of soft tissues.

For the tasks of precision low-trauma surgery, an important parameter is not only the depth of a single removed layer, but also the accuracy with which the tissue is removed to a given depth. It is clear that when the biological tissues are evaporated using the scanning method, the surface of the evaporated zone is uneven, which is primarily caused by the scanning method itself in the form of serial tissue cuts. This can be seen in photographs of the sections of the evaporated zone of the myocardial samples. It is clear that at sufficiently large distances between the hatching lines, there will be a maximum surface roughness that will represent individual cuts. As the model shows, when the distance between strokes decreases, the cutting zone of individual strokes overlaps and the surface is smoothed due to the summation of individual cut profiles (Eq. (10)). This is clearly demonstrated in Fig. 1 that shows the profiles of the evaporated zone obtained by calculation (Fig. 7).

Let us take the surface roughness $\Delta H = H_{max} - H_{min}$ as a characterizing parameter, where H_{min} is the minimum depth in the evaporation zone. Fig. 8 shows the relationship between the roughness of the evaporated zone and the scanning speed at d = 0.445 mm. The same figure shows the calculation curve, which is also in good agreement with experiment.

At the same time, the experiments on cardiac muscle have shown that the magnitude of roughness as $\Delta H = H_{max}–H_{min}$ at smaller parameters d remains quite large, while the model predicts a fairly rapid decrease in roughness with decreased distance d. For example, as shown in Fig. 7, the surface roughness at d = 0.15 mm is ΔH = 150 μm, while the experiments give the roughness of about 400–600 μm (see Fig. 2b). Apparently, this is due to the fact that the roughness of the evaporated zone is determined by other factors that are not taken into account in the model. Firstly, the amount of roughness may strongly depend on the shape of profile $h(x)$ of the individual cut. The model uses a Gaussian profile shape. The superposition of several sequential Gaussian profiles leads to noticeable smoothing due to the Gaussian tail.

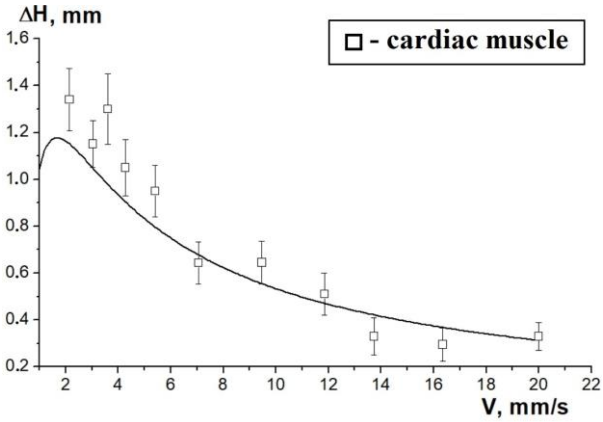

Fig. 8 The relationship between the roughness of the evaporated zone and the scanning speed at d = 0.445 mm. The black curve is the calculation.

With the shape of a separate channel $h(x)$ with sharper boundaries, such smoothing will no longer be observed. Secondly, the removal of tissue from the impact zone occurs by micro-explosions due to local overheating of water that are accompanied by tissue ruptures. This may lead to additional roughness of the resulting surface. Therefore, description of the roughness at small values of d requires a separate consideration.

It should be noted that almost all soft tissues with high water content have similar characteristics [25, 26]: density, heat capacity, thermal diffusivity, absorption coefficient at a wavelength of 10.6 μm. Such closeness of characteristics is due to the high water content. These characteristics can directly affect the threshold for the onset of laser evaporation. But in our work, we study evaporation under conditions significantly exceeding this threshold. Under such conditions, the main role in the energy balance is played by the evaporation of water, which is 70−80% or more. In this regard, the resulting evaluation formulas do not contain any specific characteristics of the biotissue except for density and thermal diffusivity.

However, tissues with a high water content may differ in mechanical and strength properties. Note that the tensile strength of soft water-containing tissues can vary from 0.01 MPa to 10 MPa. For example, the tensile strength of heart muscle is 0.04 MPa, while the strength of cartilage tissue, which also belongs to tissues with a high water content (80%), is up to 10 MPa [27, 28]. Experiments on biomodels of agar and heart muscle showed good agreement with the calculation. Therefore, it can be assumed that the proposed model can be used to estimate the depth of evaporation of other soft tissues with high water content and low tensile strength. The relationship between the mechanical and strength properties of tissues and the depth of evaporation by continuous laser radiation can be the subject of separate studies.

5 Conclusions

The features of laser evaporation of biomodels based on agar and pig tissues *in vitro* during two-coordinate scanning of continuous CO_2 laser radiation at the wavelength of 10.6 μm have been investigated both experimentally and numerically. The evaporation depth and the features of the formed surface of the evaporated area were studied for different impact modes: (1) radiation power, (2) scanning speed of the laser beam, and (3) hatching filling densities of the scanned area. It has been shown that the evaporation depth of the agar samples with 85% water practically coincides with the depth of evaporation of pig tissue samples. The agar samples can serve as good biomodels in evaluating the effectiveness of laser layer-by-layer evaporation of soft tissues. The proposed semi-empirical model of laser evaporation of soft biological tissues with high water content is based on the energy balance and the evaporative mechanism of biological tissue removal. The model allows calculating the average depth of the evaporated zone, as well as the depth of individual cuts and the unevenness of the fabric surface with a sufficiently low density of filling the scanning zone with hatching. The study has demonstrated a good correlation between the experimental data and the data obtained with the proposed model.

The study was carried out within the state task of the NRC “Kurchatov Institute”.

Disclosures

The authors declare that they have no conflict of interest.

References

1. G. Maza, A. Sharma, “Past, present, and future of robotic surgery,” Otolaryngologic Clinics of North America 53(6), 935–941 (2020).
2. J. Han, J. Davids, H. Ashrafian, A. Darzi, D. S. Elson, and M. Sodergren, “A systematic review of robotic surgery: From supervised paradigms to fully autonomous robotic approaches,” Robotics Computer Surgery 18(2), e2358 (2022).
3. I. O. Gritskov, A. A. Vitoslavskii, K. A. Kryazheva, A. O. Vasil’ev, K. B. Kolontarev, and D. Yu. Pushkar’, “Robotic systems in surgery,” Biomedical Engineering 55(5), 365–369 (2022).

4. Y. Y. Juo, A. Abiri, J. Pensa, S. Sun, A. Tao, J. Bisley, W. Grundfest, and E. Dutson, "Center for advanced surgical and interventional technology multimodal haptic feedback for robotic surgery," 17 Chapter in Handbook of Robotic and Image-Guided Surgery, M. H. Abedin-Nasab (Ed.), Elsevier, 285−301 (2020). ISBN: 978-0-12-814245-5.
5. U. Paasch, M. Haedersdal, "Laser systems for ablative fractional resurfacing," Expert Review of Medical Devices 8(1), 67–83 (2011).
6. A. Aslam, T. S. Alster, "Evolution of laser skin resurfacing: from scanning to fractional technology," Dermatologic Surgery 40(11), 1163–1172 (2014).
7. R. Colasanti, L. Giannoni, S. Dallari, V. Liverotti, D. Aiudi, A. Di Rienzo, F. Rossi, and M. Iacoangeli, "Application of a scanner-assisted carbon dioxide laser system for neurosurgery," World Neurosurgery 153, e250–e258 (2021).
8. A. R. Padalhin, "Lasers and robots: recent developments in transoral laser and transoral robotic surgery," Medical Lasers 9(2), 103–109 (2020).
9. H. C. Lee, N. E. Pacheco, L. Fichera, and S. Russo, "When the end effector is a laser: a review of robotics in laser surgery," Advanced Intelligent Systems 4(10), 2200130 (2022).
10. A. Acemoglu, L. Fichera, I. E. Kepiro, D. G. Caldwell, and L. S. Mattos, "Laser incision depth control in robot-assisted soft tissue microsurgery," Journal of Medical Robotics Research 02(03), 1740006 (2017).
11. S. Stopp, D. Svejdar, E. Von Kienlin, H. Deppe, and T. C. Lueth, "A new approach for creating defined geometries by navigated laser ablation based on volumetric 3-d data," IEEE Transactions on Biomedical Engineering 55(7), 1872–1880 (2008).
12. L. Fichera, D. Pardo, P. Illiano, J. Ortiz, D. G. Caldwell, and L. S. Mattos, "Online estimation of laser incision depth for transoral microsurgery: approach and preliminary evaluation," Robotics Computer Surgery 12(1), 53–61 (2016).
13. G. Ma, R. Prakash, B. Mann, W. Ross, and P. Codd, "3D Laser-and-tissue agnostic data-driven method for robotic laser surgical planning," in 2023 IEEE/RSJ International Conference on Intelligent Robots and Systems (IROS), Detroit, MI, USA (2023).
14. D. A. Hashimoto, G. Rosman, D. Rus, and O. R. Meireles, "Artificial intelligence in surgery: promises and perils," Annals of Surgery 268(1), 70–76 (2018).
15. F. Partovi, J. A. Izatt, R. M. Cothren, C. Kittrell, J. E. Thomas, S. Strikwerda, J. R. Kramer, and M. S. Feld, "A model for thermal ablation of biological tissue using laser radiation," Lasers in Surgery and Medicine 7(2), 141–154 (1987).
16. A. L. McKenzie, "A three-zone model of soft-tissue damage by a CO 2 laser," Physics in Medicine & Biology 31(9), 967–983 (1986).
17. A. M. Sagi-Dolev, "Heating of biological tissue by laser irradiation: temperature distribution during laser ablation," Optical Engineering 31(7), 1425 (1992).
18. G. L. LeCarpentier, M. Motamedi, L. P. McMath, S. Rastegar, and A. J. Welch, "Continuous wave laser ablation of tissue: analysis of thermal and mechanical events," IEEE Transactions on Biomedical Engineering 40(2), 188–200 (1993).
19. R. Dua, S. Chakraborty, "A novel modeling and simulation technique of photo–thermal interactions between lasers and living biological tissues undergoing multiple changes in phase," Computers in Biology and Medicine 35(5), 447–462 (2005).
20. V. Venugopalan, N. S. Nishioka, and B. B. Mikić, "Thermodynamic response of soft biological tissues to pulsed infrared-laser irradiation," Biophysical Journal 70(6), 2981–2993 (1996).
21. A. K. Dmitriev, A. N. Konovalov, V. N. Kortunov, and V. A. Ulyanov, "Diagnostics of layer-by-layer biotissue evaporation in the process of two-coordinate scanning by a laser beam for precision surgery," Journal of Biomedical Photonics & Engineering 9(2), 020302 (2023).
22. G. M. Hale, M. R. Querry, "Optical constants of water in the 200-nm to 200-μm wavelength region," Applied Optics 12(3), 555 (1973).
23. V. M. Gordienko, A. N. Konovalov, Yu. Ya. Putivskii, N. N. Kurochkin, and V. I. Savin, "Investigation of the dynamics of laser-induced explosive boiling of water using the autoheterodyning scheme," High Temperature 36(5), 789−795 (1998) [in Russian].
24. A. K. Dmitriev, A. N. Konovalov, V. N. Kortunov, and V. A. Ulyanov, "Doppler diagnostics of laser evaporation of biological tissues," Journal of Laser Applications 34, 041201 (2022).
25. V. Tuchin (Ed.), "Tissue Optics. Light Scattering Methods and Instruments for Medical Diagnosis," SPIE (2007). PDF ISBN: 9780819481061.
26. K. Giering, O. Minet, I. Lamprecht, and G. Müller, "Review of Thermal Properties of Biological Tissues," in Laser-Induced Interstitial Thermotherapy, G. Muller, A. Roggan (Eds.), SPIE Press, Washington, USA, 45−65 (1995).
27. J. T. Walsh, T. F. Deutsch, "Pulsed CO2 laser ablation of tissue: effect of mechanical properties," IEEE Transactions on Biomedical Engineering 36(12), 1195−1201 (1989).
28. V. A. Berezovskii, N. N. Kolotilov, Biophisisheskie characteristiki tkanei cheloveka. Spravochnik, Kiev, Naukova dumka, (1990) [in Russian]. ISBN: 5120013740.